Reconstruction objects hidden in scattering medium using microlens array

David Abookasis and Joseph Rosen
Ben-Gurion University of the Negev
Department of Electrical and Computer Engineering
P. O. Box 653, Beer-Sheva 84105, Israel

ABSTRACT

We propose and experimentally demonstrate a new reconstruction method of objects hidden in scattering medium. The object (chicken bone) hidden between two slabs of chicken breast is reconstructed from many speckled images formed by a microlens array (MLA). Each microlens from the array projects a small different speckled image of the hidden object onto a CCD camera. The entire noisy images from the array are digitally processed to yield the hidden object. Following this method, a different algorithm implemented on the same optical system has been developed. This modified algorithm, based on the point-source reference method improve the resolution of the previously method. Experimental results are presented that demonstrate our theory and possible applications of this technique are discussed.

Keywords: Scattering Medium, Speckled Images, Microlens Array, Optical Data Processing.

1. INTRODUCTION

In recent years many efforts have been devoted to finding ways for reconstruction objects embedded in a scattering medium using optical means. This topic has potential application in medical diagnosis since it is safe, noninvasive and low-cost, compared with the conventional radiation techniques. The tendency in the optical imaging techniques is to work in the spectral window (600-1300nm) where the absorption of light by most soft tissues is low enough for photons to penetrate deeply into these tissues. Many different reconstruction techniques have been proposed to enhance the ability of the optical imaging. Each of these technologies has particular advantages and disadvantages[1].

In this work we propose a new scheme of seeing through scattering medium inspired by the fly's visual system. The visual system of the fly is composed of multifaceted eyes, shown in Fig.1. In addition the fly is equipped with a neural superposition system. This means that several identical images from several facets are superposed together to a single common image by neural connections of the photoreceptors.[2] Emulating the fly's eye principle, i.e. superposing multiple images from many imaging channels, enables us to see general objects hidden behind scattering layers.

The proposed system shown in Fig. 2 is based on a simple optical imaging containing microlens array (MLA). Each lens of the array projects a different speckled image on a digital camera through imaging lens. In the computer the set of speckled images from the entire array are first shifted to a common center and then accumulated to a single average
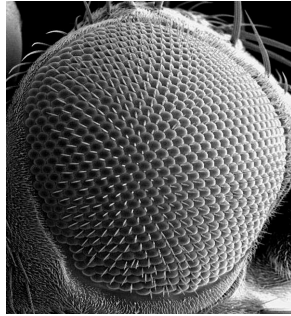
Figure 1: Picture of the fly's compound eye.

picture. In the second algorithm to be presented here, each image is Fourier transformed jointly with an image of a speckled point-like source captured under the same conditions. The set of the squared magnitude of the Fourier transformed pictures are accumulated together to a single average picture. This final picture is again Fourier transformed, resulting a reconstruction of the hidden object.
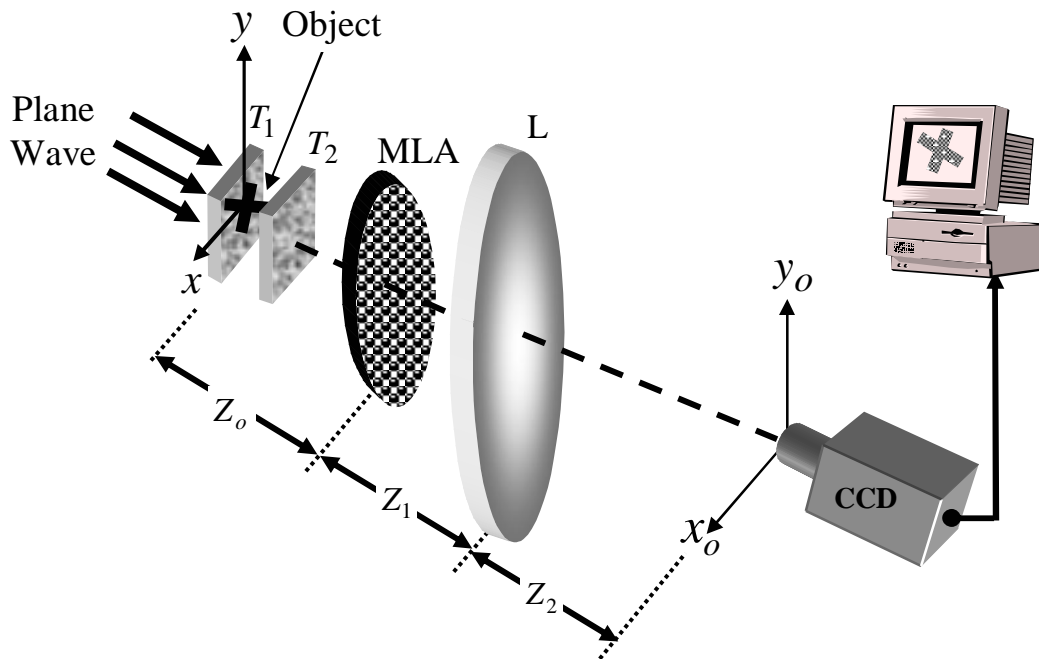
Figure 2: Schematic of the optical system.

2. OPTICAL IMAGING BY SPECKLE ENSEMBLE

Following is the mathematical description of both algorithms. Without the scattering layers, the illuminated coherently system is characterized by a relatively narrow point spread function (PSF) $h_o(x,y)$[3]. This PSF is calculated conventionally as an inverse Fourier transform of the aperture of a single micro-lens. In the present case, the micro-lens imposes the system bandwidth because its numerical aperture is smaller than that of the imaging lens L. Next, we

consider the effect of the back scattering layer T_1. This layer diffuses the light such that each micro-lens gets almost uniformly part of the illumination. In addition, because of the randomness of the medium T_1 and its uniformity, the object is multiplied by a random phase function with almost constant magnitude. The entire system is modeled as an array of several identical imaging systems, all with the same PSF given by $h_o(r)$, where $r=(x,y)$ is the position vector. In each imaging channel the input function is $t(r)=A(r)\exp[i\phi(r)]$, where $A(r)$ stands for the object amplitude function and $\phi(r)$ is a random phase function induced by layer T_1. The image intensity at the k-th coherently illuminated channel is given by[3]

$$I(r_o) = |t(r_o) * h_o(r_o)|^2 \qquad (1)$$

where the asterisk denotes two-dimensional convolution, and $r_o=(x_o,y_o)$ is the position vector on the output plane. $I(r_o)$ of Eq. (1) is the diffraction limited image of the squared function of the object, $|A(r_o)|^2$. The goal of the following proposed process is to produce intensity distribution as close as possible to $I(r_o)$.

When the front scattering layer T_2 is introduced into the system, the output image is distorted such that the object cannot be recognized. Since each micro-lens observes the object through a different transverse cross-section of the scattering layer, each k-th micro-lens together with the lens L create a linear system characterized by a different random PSF $h_k(r)$. Therefore, the output intensity pattern in each coherently illuminated k-th channel is given by $\tilde{I}_k(r_o) = |t(r_o) * h_k(r_o)|^2$. It is assumed that although each PSF $h_k(r)$ is a random function, wider than $h_o(r)$, the ensemble average PSF over the entire K channels satisfies the relation:

$$\frac{1}{K}\sum_k h_k(r) \cong h_o(\mathrm{r}) \qquad (2)$$

This assumption is valid for scattering mediums satisfying statistics of Rytov model with weak phase modulation and Born model[4]. Having the set of K speckled images $\{\tilde{I}_k(r_o)\}$, we first center each one of them and then sum them to a single average image given by,

$$S(r_o) = \frac{1}{K}\sum_k |t(r_o) * h_k(r_o)|^2 \qquad (3)$$

In order to show that this ensemble average is approximately equal to the diffraction-limited image given by Eq. (1), the convolution of Eq. (3) is explicitly written and the order of integration and summation is interchanged as follows

$$S(r_o) = \int_{-\infty}^{\infty}\int_{-\infty}^{\infty} t(r_1)t^*(r_2)\left[\frac{1}{K}\sum_k h_k(r_o - r_1)h_k^*(r_o - r_2)\right]dr_1 dr_2, \qquad (4)$$

where the superscript asterisk denotes the complex conjugate. The internal averaging in Eq. (4) can be separated to two summations, one includes all pairs of functions $h_k(r)$ shifted by different distances, i.e. $r_1 \neq r_2$. The ensemble average in this case is calculated on the multiplication of two uncorrelated random variables, and hence this ensemble average is equal to the multiplication of their ensemble averages. The second summation represents all the pair functions shifted equally, i.e. $r_1=r_2$. This latter sum is the ensemble average on the set of random functions $\{|h_k(r)|^2\}$ which, based on Eq. (2) is given by $\frac{1}{K}\sum_k |h_k(r)|^2 \cong |h_o(r)|^2 + \sigma^2(r)$, where σ^2 is the variance of the random set $\{h_k(r)\}$, defined as $\sigma^2(r) = \frac{1}{K}\sum_k |h_k(r) - h_o(r)|^2$. Under the above assumption of weak scatterer, we assume that this variance along r is much smaller than $\underset{r}{MAX}|h_o(r)|^2$, but it is not negligible. Based on the above arguments, Eq. (4) becomes

$$S(r_o) \cong |t(r_o) * h_o(r_o)|^2 + |t(r_o)|^2 * \sigma^2(r_o) \qquad (5)$$

The first term of Eq. (5) is approximately the desired diffraction-limited image given by Eq. (1). The second term is a convolution between the object and the variance functions. Clearly $\sigma^2(r)$ is wider than $h_o(r)$ because the scattering layer broaden the diffraction-limited image of a point. Therefore, we conclude that the second convolution in Eq. (5) blurs the diffraction-limited image of the object. The value of this blurring term is determined by the average value of the variance $\sigma^2(r)$. The contrast and the sharpness of the reconstructed object are inversely dependent on the variance.

In contrast to the above algorithm, the second algorithm makes use of the point-source reference in order to prevent the need to shift the speckled images toward a common center. Therefore, in addition to the speckled images of the object, we record speckled images of a point-like object. After collecting all the object's speckled images by the MLA, the setup is illuminated by the point-source, and speckled patterns of this point-source, through the same number of channels, are also captured by CCD. Each sub-image of the speckled object with a corresponding sub-image of the speckled point-like source are placed together side by side in the computer, and jointly Fourier transformed. The squared magnitudes of the jointly transformed pictures are accumulated in order to compose a single average joint power spectrum. Object reconstruction is achieved by another Fourier transform (FT) of this average spectrum. As a result, the final image is close to a cross-correlation between the object function and a narrow point-like source. The main idea of this technique is that the relative locations between the speckle patterns do not have any influence on the reconstruction result. The algorithm relay on the assumption that in every channel, the object and the point-like reference suffer from the same scattering. Therefore they are both shifted by the same amount relatively to other channels, but the mutual distances between the speckled images of the object and the point-like reference in the entire channels are the same. Let us describe these steps more rigorously. Let the function $f_k(x,y)$ represents intensity of the k-th speckled image of the same embedded object function $t(x,y)$. The function $r_k(x,y)$ stands for the k-th intensity of the speckled image of the point-like function approximated by the Dirac Delta function $\delta(x,y)$. Under coherent illumination, both functions $t(x,y)$ and $\delta(x,y)$ are convolved with a randomly speckled k-th point-spread function (PSF), $h_k(x,y)$, as the following

$$f_k(x,y) = \left| t(x,y) * h_k(x,y) \right|^2, \tag{6}$$

$$r_k(x,y) \cong \left| \delta(x,y) * h_k(x,y) \right|^2 = \left| h_k(x,y) \right|^2, \qquad k = 1,2,..., K$$

where K is the total number of imaging channels. In the computer the reference and the object speckled images are combined such that both are situated in the same plane, separated by a distance (a,b) from each other. The accumulated intensity pattern of the entire joint power spectrums is

$$I(u,v) = \frac{1}{K} \sum_k I_k(u,v)$$

$$= \frac{1}{K} \sum_k \left| \mathfrak{F}_{2D} \{ f_k(x + x_k + a/2, y + y_k + b/2) + r_k(x + x_k - a/2, y + y_k - b/2) \} \right|^2$$

$$= \frac{1}{K} \sum_k |F_k(u,v)|^2 + |R_k(u,v)|^2 + F_k^*(u,v)R_k(u,v)\exp\left[-i2\pi(au+bv)\right]$$

$$+ F_k(u,v)R_k^*(u,v)\exp\left[i2\pi(au+bv)\right], \tag{7}$$

where (u,v) are the spatial frequency coordinates, $\mathfrak{F}_{2D}$ denotes a 2-D FT operation, F_k,R_k are the FTs of f_k,r_k, respectively and (x_k,y_k) is the k-th random shift resulting from light propagation through the k-th portion of the scattering layer. Since the light from the reference and the object suffers from the same scattering in each channel, they are both shifted by the same distance in each k-th channel. Therefore, the magnitude expression in Eq. (7) eliminates

the linear phase factor resulting from the shift (x_k, y_k). Another FT of the expression of Eq. (7) yields the output function,

$$C_{out}(\xi,\eta) = \frac{1}{K} \sum_k \left[f_k(\xi,\eta) \otimes f_k(\xi,\eta) + r_k(\xi,\eta) \otimes r_k(\xi,\eta) \right]$$
$$+ \left[\frac{1}{K} \sum_k r_k(\xi,\eta) \otimes f_k(\xi,\eta) \right] * \delta(\xi - a, \eta - b)$$
$$+ \left[\frac{1}{K} \sum_k f_k(\xi,\eta) \otimes r_k(\xi,\eta) \right] * \delta(\xi + a, \eta + b), \tag{8}$$

where (ξ,η) are the coordinates of the output plane and $\otimes$ denotes correlation operator. It is clear from Eq. (8) that three spatially separated Fourier orders can be observed. The second and the third terms at the points $(\pm a, \pm b)$ are of interest here, corresponding to the convolution between the object $t(\xi,\eta)$ with narrow functions, as discussed below. Therefore, the object image is retrieved by observing the pattern at the vicinity of the points (a,b), or $(-a,-b)$. Let us now, for simplicity, concentrate only in the third term of Eq. (8), expected to yield the reconstructed image at the point (a,b). Substituting Eqs. (6) and Eq. (2) into the third term of Eq. (8), and following a straightforward algebra, the third term becomes,

$$C_3(\xi - a, \eta - b) = \frac{1}{K} \sum_k \left| t(\xi,\eta) * h_k(\xi,\eta) \right|^2 \otimes \left| h_k(\xi,\eta) \right|^2 \tag{9}$$
$$\cong \left| t(\xi,\eta) * h_o(\xi,\eta) \right|^2 \otimes \left| h_o(\xi,\eta) \right|^2 + \sigma^2(\xi,\eta) * \left| t(\xi,\eta) \right|^2 \otimes \left| h_o(\xi,\eta) \right|^2$$
$$+ \sigma^2(\xi,\eta) \otimes \left[\left| t(\xi,\eta) * h_o(\xi,\eta) \right|^2 + \left| t(\xi,\eta) \right|^2 * \sigma^2(\xi,\eta) \right]$$

The first term of Eq. (9) is the desired image of the embedded object. As seen from this term, the image is obtained by convolving the object function $t(\xi,\eta)$ twice with the diffraction-limited PSF $h_o(\xi,\eta)$. Therefore, independently of the scattering, this imaging method has an inherent loss of resolution because of the double convolution with the PSF $h_o(\xi,\eta)$. The rest of the terms of Eq. (9) are convolution between the object and the variance function $\sigma^2(\xi,\eta)$ as defined above. Again, since the variance $\sigma^2(\xi,\eta)$ is wider than $h_o(\xi,\eta)$ the terms of convolution with the variance function in Eq. (9) blurs the diffraction-limited image of the object and the value of these blurring terms is determined by the average value of the variance.

3.   EXPERIMENTAL RESULTS

To demonstrate the proposed technique with the first algorithm, an opaque object made of chicken bones in a shape of a cross-junction with the size of $9\times9mm$ was embedded between two layers of chicken breast separated from each other by a distance of $12mm$. The thickness of the rear tissue T_1 was about $3mm$, whereas the thickness of the front tissue T_2, was about $8mm$. The reduced scattering coefficient of the tissues of $\mu_s'=4.5\pm0.3cm^{-1}$ was measured by the method proposed in Ref. 5. Assuming the anisotropy factor is $g=0.965$ (see Ref. 6), the scattering coefficient becomes $\mu_s = \mu_s'/(1-g) = 128 \pm 9 cm^{-1}$. The rear tissue T_1 was illuminated by a collimated plane wave of $35mW$ He-Ne laser with $\lambda=632.8nm$ wavelength. The MLA (Adaptive Optics, 0500-3.3-H), placed a distance of $Z_o=160mm$ from the object, was composed of 115×100 hexagonal refractive lenses. Only the central $132=12\times11$ lenses were used in the present experiments. The radius of each micro-lens is $r=250\mu m$ and its focal length equal to $3.3mm$. Under these conditions the optical system without the tissues can resolve a minimum size of $\lambda Z_o/r \cong 0.4mm$. The resolution can be improved using lenses with larger apertures. However, this change may increase the total view angle of the system and thus the various channels may image different perspectives with different shapes of the same object. The image plane

of the MLA was projected onto the CCD plane by a single spherical imaging lens L, with a 300mm focal length. The distance Z_1 and Z_2 shown in Fig.2 were 520mm and 710mm, respectively. In the experiment we used a CCD camera (PCO Scientific, 230XS1574) with 1280(H) ×1024(V) pixels, within 8.6×6.9mm square active area.

Figure 3 show the array of all speckled images recorded by the CCD, whereas the white lines indicate the image area contributed by each single lens. These lines were synthetically added, by the reconstruction program, on the original captured picture only for clarity. From this figure it is clear that the original object cannot be recognized from any image of the 132 different blurred images.
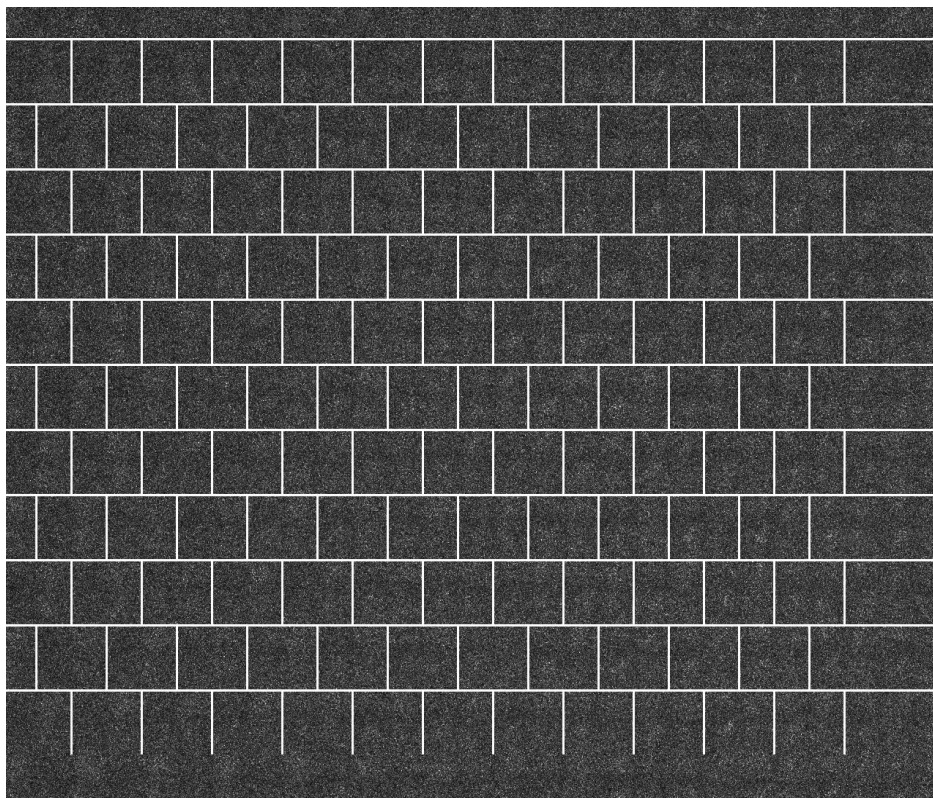
Figure 3: 12×11 blurred images recorded by the CCD when the cross-junction sign is embedded between the two slabs of chicken breast.

Each blurred sub-image of the size 96×84 pixels from the array was extracted from the matrix, and shifted toward a common center. We calculated the center of gravity of each contrast-inverted blurred cloud of the entire set of 132 blurred images. The center of gravity is considered as the true center of the object in each frame, and accordingly all the images are centered to have the same center of gravity. We assume that the angular difference between the most extreme view points is small enough (less than 3° in the present experiment) to neglect the differences between all the various perspectives of the object observed from the various channels. Although the lateral shift of the object image depends on the longitudinal position of the object in the scattering layers (denoted as Z_o in Fig. 2), it does not mean that one should know the longitudinal position of the object in the scattering layers in prior to image the object. The algorithm of calculating the blurred image's center of gravity yields the various positions of the object in all the channels regardless of object's longitudinal position. The reconstruction process from Fig.3 is shown in Fig. 4.

Figure 4: The reconstructed object.

To demonstrate the proposed technique with the second algorithm, a transparent object in the form of the letter **V** with the size of $7 \times 11mm$ was embedded again between two layers of chicken breast separated from each other by a distance of $12mm$. The thicknesses of the layers, the back T_1 and the front T_2, were about $3mm$ and $4mm$, respectively. The scattering coefficient value of the layers is the same as before. The rear tissue T_1 was illuminated by the He-Ne laser and speckle images were taken with the MLA placed at a distance $Z_o=160mm$ from the object. The MLA image plane is then imaged by the lens L onto a CCD camera. Figure 5 shows several elemental images, out of 132 speckled images, of the point-source [Fig. 5(a)] and of the object [Fig. 5(b)] as recorded by the CCD.

(a)   (b)
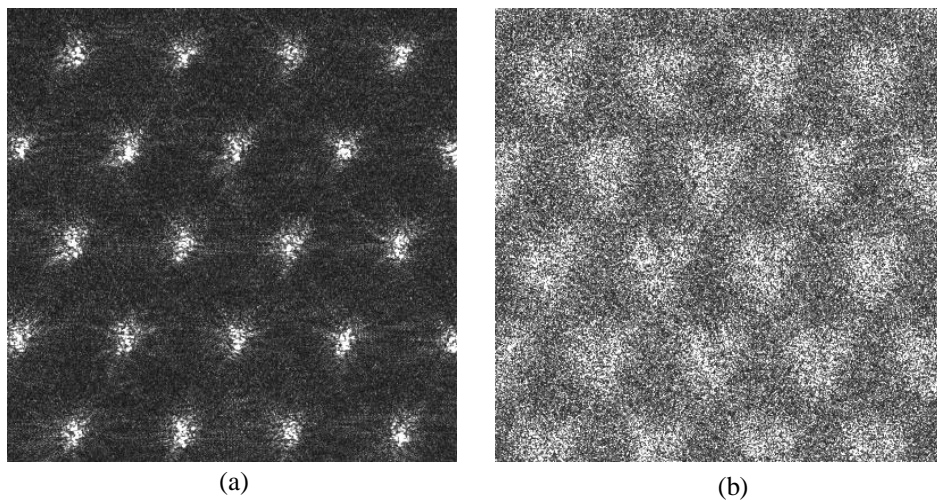
Figure 5: 22 projections, out of 132 speckled images of (a) the point-source reference and (b) the object.

In the computer each sub-image of the array originated from the object is combined with the corresponding sub-image of the array originated from the point-source. The point-source was created by placing a pinhole attached to the tissue T_1 from the side illuminated by the laser. The pinhole is located a short distance behind layer T_1 and the object, that enables us to neglect the mutual movement between the point and the object along the full angular range of ~3° of the MLA. Thus from practical point of view the point source and the object are considered as located at the same location in space. The light from the pinhole goes through the object such that the embedded object does not need to be removed. Although this method becomes more complicated due to the double recording process, the increase of accuracy justifies its use. Each enlarged input plane, containing the speckled point source aside with the speckled object, is Fourier transformed. The square magnitude of each channel's spectrum is accumulated with all the others. This average joint power spectrum is then Fourier transformed again to the output correlation plane. The three orders of the correlation plane containing the revealed image of the object in both two side-lobes can be clearly seen in Fig. 6.
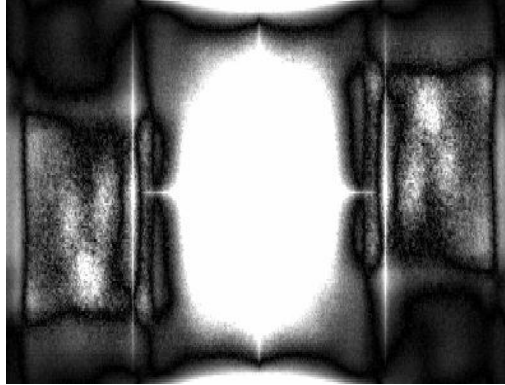
Figure 6: Experimental results of the second algorithm. The desired image of the hidden object is recovered on both side-lobes.

Fig. 7(a) shows the recovered image of the letter **V**, taken from the left side-lobe of Fig. 6. For comparison, Fig. 7(b) shows the average image of the letter **V** without the scattering layer T_2. The effect of extending the object in Fig. 7(a) in comparison to Fig. 7(b) is clearly seen. This phenomenon is due to the double convolution with the PSF h_o in Fig. 7(a) in contrast to a single convolution in Fig. 7(b). The image obtained using the first algorithm is shown in Fig. 7(c). From comparison Figs. 7(a) and 7(c), it seems that imaging by cross-correlation with a point reference [Fig. 7(a)] yields a better resolution than imaging by the shift-and-add algorithm [Fig. 7(c)]. The resolution improvement is quantified by comparing the deepness of the notch between the lines of the letter **V** in the results. Our measurements indicate that the notch in Fig. 7(a) is, in average, 30% deepest than the notch of Fig. 7(c).

(a) (b) (c)
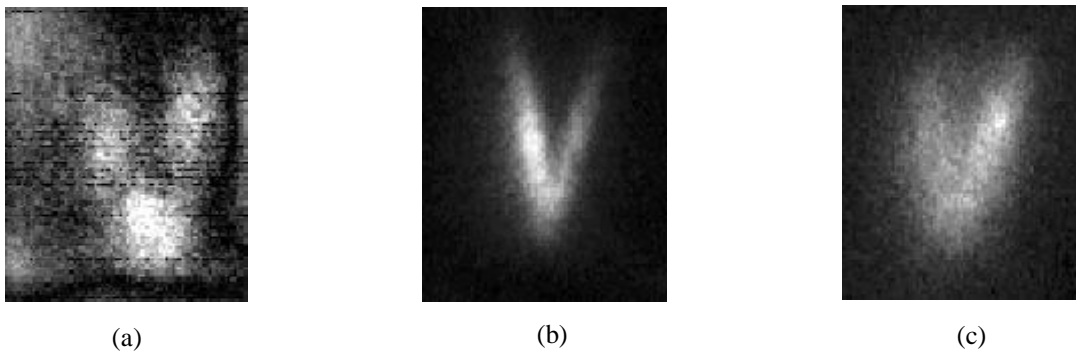
Figure 7: (a) The left-side-lobe from Fig. 6. (b) The average picture of the entire array when the letter **V** is positioned in front of layer T_1 and the layer T_2 is removed. (c) The recovered image of the letter **V** obtained by the shift-and-add algorithm.

4. DISCUSSION AND CONCLUSIONS

In conclusion, we have presented and successfully demonstrated a new process for reconstruction object in scattering medium. Two kinds of image processing techniques have been demonstrated, each of which has its own advantage and weakness.

In order to verify the need of using coherent light, an experiment of imaging through the same scattering layer with a Halogen lamp was conducted. Averaging over the entire recorded pictures yields unrecognizable picture since the object is illuminated by a bunch of plane waves with many different angles. The effect on the output image in each channel is an accumulation of many blurred images of the object shifted randomly from the true object center. Therefore, the result in each imaging channel will be smoothly blurred unrecognizable image of the object. Accumulating these images along the all channels won't enable to see through the scattering medium.

In another experiment we investigated if lateral averaging over high resolved image is equivalent to averaging over many low resolved images as done in the experiment with the MLA. For this, we removed the MLA and imaged the object onto the CCD with 48 times better resolution than in the setup with the MLA. Then, every successive rectangle of 48×48 pixels on the image matrix was averaged. Results have not produced any recognizable image of the object. This shows that the procedure of averaging the low resolved MLA images is significantly superior over the averaging a single high resolved image.

The weakness of the present techniques is the relatively low spatial bandwidth product of the diffraction limited system. The use of a small aperture lens at each imaging channel reduces both the field of view and the system's bandwidth. However, this drawback seems as a reasonable penalty to pay for the ability to see through scattering medium in a simple and robust way. The advantages of the method are relative simplicity, low cost, fast operation and the need of low power CW laser illumination. Because of all these advantages our system has a high potential in versatile imaging applications, especially in the medical diagnostic.

REFERENCES

1. J. C. Hebden, S. R. Arridge and D. T. Delpy, "Optical imaging in medicine: I. Experimental techniques," *Phys. Med. Biol*. **42**, 825 (1997).
2. M. F. Land, and D.-E. Nilsson, *Animal Eyes* (Oxford Univ. Press, New York, 2002), 125-155.
3. J. W. Goodman, *Introduction to Fourier Optics,* 2nd ed. (McGraw-Hill, New York, 1996), 126-130.
4. T. Vo-Dinh *ed.*, Biomedical Photonics Handbook (CRC Press, Boca Raton 2003), **21**-8.
5. L. Wang, and S. L. Jacques, "Use of a laser beam with an oblique angle of incidence to measure the reduced scattering coefficient of a turbid medium," *Appl. Opt*. **34**, 2362-2366 (1995).
6. W.-F. Cheong, S. A. Prahl, and A. J. Welch, "A review of the optical properties of biological tissues," *IEEE J. of Quant. Elect*. **26**, 2166-2185 (1990).